Ca^{2+} Transport Properties of Ionophores A23187, Ionomycin, and 4-BrA23187 in a Well Defined Model System

Warren L. Erdahl,*‡ Clifford J. Chapman,*‡ Richard W. Taylor,§ and Douglas R. Pfeiffer*‡
*Department of Medical Biochemistry, The Ohio State University, Columbus, Ohio 43210, §Department of Chemistry, University of Oklahoma, Norman, Oklahoma 73019, and ‡Hormel Institute, University of Minnesota, Austin, Minnesota 55912 USA

ABSTRACT Models for the electroneutral transport of Ca^{2+} by ionophores A23187, ionomycin, and 4-BrA23187 have been tested in a defined system comprised of 1-palmitoyl-2-oleoyl-*sn*-glycerophosphatidylcholine vesicles prepared by freeze-thaw extrusion. Quin-2-loaded and $CaCl_2$-loaded vesicles were employed to allow the investigation of transport in both directions. Simultaneous or parallel measurements of H^+ transport and membrane potential, respectively, indicate that for any of these ionophores, electrogenic transport events do not exceed 1 in 10,000 when there is no preexisting transmembrane potential. When a potential of ~150 mV is imposed across the membrane, transport catalyzed by A23187 remains electroneutral; however, for ionomycin and 4-BrA23187, approximately 10% of transport events may be electrogenic. The defined vesicle system has also been utilized to determine how the rate of Ca^{2+} transport varies as a function of ionophore and Ca^{2+} concentration and with the direction of transport. Some aspects of the results are unexpected and should be considered by investigators using ionophores in biological systems. These include the apparent failure of these compounds to fully equilibrate Ca^{2+} with a high affinity Ca^{2+} indicator when these species are separated by a membrane, rates of transport that vary markedly with the direction of transport, and extents of transport that are a function of ionophore concentration. At least some of these unexpected behaviors can be explained by a strong influence of ΔpH on forward and reverse transport kinetics. In the case of A23187, the data also give some initial insights into the relationship between formation of the transporting species and the entry of this species into the membrane hydrophobic region.

INTRODUCTION

The ionophores A23187 and ionomycin are used widely to investigate the regulatory activities and metabolism of Ca^{2+} in biological systems. Effects of these compounds are routinely attributed to the electrically neutral exchange of Ca^{2+} for $2H^+$ or for another divalent cation (i.e., Mg^{2+}). However, the evidence that this is the only transport activity of interest is not extensive. Regarding selectivity for Ca^{2+}, it is now clear that both compounds form complexes with a variety of divalent cations encountered in biological systems in addition to Ca^{2+} and Mg^{2+} (Kauffman et al., 1982; Bolte et al., 1982; Taylor et al., 1985; Chapman et al., 1987; Divakar and Easwarn, 1987; Antonenko and Yaguzhinsky, 1988; Suzuki et al., 1988; Albrecht-Gary et al., 1989; Chapman et al., 1990; Stiles, et al., 1991). The pattern of stability constants for both ionophores obeys the extended Irving-Williams series, indicating no unusual complexation selectivity for Ca^{2+} (Chapman et al., 1990; Stiles et al., 1991). Complexes between A23187 and monovalent or trivalent cations are well known (Pfeiffer et al., 1974; Puskin and Gunter, 1975; Pfeiffer and Lardy, 1976; Pfeiffer et al., 1978; Tissier et al., 1979) and apparently also exist with ionomycin (Liu and Hermann, 1978; Suzuki et al., 1987, 1988). Thus, the available solution equilibrium data do not support the idea that A23187 and ionomycin are highly selective as ionophores for Ca^{2+}.

Adherence to the electroneutral transport mode over a range of conditions is also open to question. In mitochondria, either ionophore acting in conjunction with the endogenous Ca^{2+} uniporter produces a charge and pH-neutral cycle of Ca^{2+} uptake and release (Reed and Lardy, 1972; Reed et al., 1975; Pfeiffer et al., 1976; Kauffman et al., 1980). They extract divalent cations from an aqueous to an organic phase in the absence of a lipophilic anion (see Taylor et al., 1983 for review) and can form neutral complexes as further indicated by solution equilibrium studies cited above, and by solution and solid state structural information (Deber and Pfeiffer, 1976; Chaney et al., 1976; Smith and Duax, 1976; Anteunis, 1977; Toeplitz et al., 1979; Anteunis and Verhegge, 1981). Thus, it is reasonable to assume that A23187 and ionomycin are capable of electroneutral transport, although this has never been demonstrated quantitatively. Furthermore, both compounds form relatively lipophilic complexes that bear a positive charge. For A23187 interacting with divalent cations these are of the type MA^+, whereas for ionomycin they are monoprotonated forms of the 1:1 species (MHI^+). Under conditions of cation concentration and pH that exist in biological systems, results from solution studies suggest that these species coexist with the neutral transporting species MA_2 and MI (Chapman et al., 1987, 1990; Stiles et al., 1991). The possibility that the charged species allows electrogenic transport modes or results in cation-anion co-transport through formation of ternary complexes has been pointed

Received for publication 7 September 1993 and in final form 10 January 1994.

Address reprint requests to Douglas R. Pfeiffer, Ph.D., The Ohio State University, Department of Medical Biochemistry, 310A Hamilton Hall, 1645 Neil Avenue, Columbus, Ohio 43210-1218. Tel: 614-292-5451; Fax: 614-292-4118.

Abbreviations used: MLV, multilamellar phospholipid vesicles; POPC, 1-palmitoyl-2-oleoyl-*sn*-glycero-phosphatidylcholine; TPP^+, tetraphenylphosphonium cation.

0006-3495/94/05/1678/16 $2.00

out (Pfeiffer and Lardy, 1974; Chapman et al., 1987, 1990; Stiles et al., 1991).

The use of electrical techniques to monitor transport by these compounds across planar lipid bilayers has not given evidence of electrogenic transport modes under specific conditions (Kafka and Holz, 1976; Wulf and Pohl, 1977; Moronne and Cohen, 1982). However, Fasolato and Pozzan (1989) have reported that Ca^{2+} transport into intact cells by either ionophore is inhibited by depolarization. Their interpretation was that both ionophores transport electrogenically across the plasma membrane. Effects of an imposed membrane potential on the rate of Ca^{2+} transport into multilamellar phospholipid vesicles (MLV) were not highly conclusive, but tended to support the possibility of an electrogenic mechanism (Fasolato and Pozzan, 1989). In view of the requirement to understand the transport mode and specificities when interpreting ionophore effects on biological preparations, we have undertaken investigation of the transport mechanisms of A23187, 4-BrA23187, and ionomycin in a well defined model system. The approach taken is to begin with previously proposed models for electroneutral transport and then determine if actual transport data are consistent with them over a range of conditions. The models of interest are shown in Fig. 1, *A* and *B* for A23187 (4-BrA23187) and ionomycin, respectively. They are composed, in either case, of eight consecutive component reactions that when taken in sum are equal to the electroneutral exchange of a divalent cation for 2 H^+ (Pfeiffer et al., 1978; Kauffman et al. 1983; Taylor et al., 1983; Sankaram et al., 1987; Fasolato and Pozzan, 1989). They are minimal models with respect to the number of steps involved, and these steps are assumed to occur at the membrane-aqueous phase interfaces. The models are consistent with what is known about the behavior of the free ionophores and their complexes in solution and in the solid state, as summarized above. They are also consistent with the data available on how these compounds interact with membranes (Case et al., 1974; Puskin et al., 1981; Brasseur et al., 1983; Kauffman et al., 1983).

In the present report, we describe the model system used to investigate cation transport kinetics and present the effects of ionophore and Ca^{2+} concentrations on the rate of Ca^{2+} transport within the system. Measurements of H^+:Ca^{2+} transport ratios and estimates of membrane potential during transport are also presented. The results are considered in terms of the behavior expected, assuming adherence to the models shown in Fig. 1.

MATERIALS AND METHODS

Reagents

Synthetic 1-palmitoyl-2-oleoyl-*sn*-glycerophosphatidylcholine (POPC) was obtained from Avanti Polar Lipids, Inc. (Alabaster, AL). Purity was confirmed by thin-layer chromatography before use. A23187, 4-BrA23187, and ionomycin were obtained from Calbiochem (LaJolla, CA) and were used

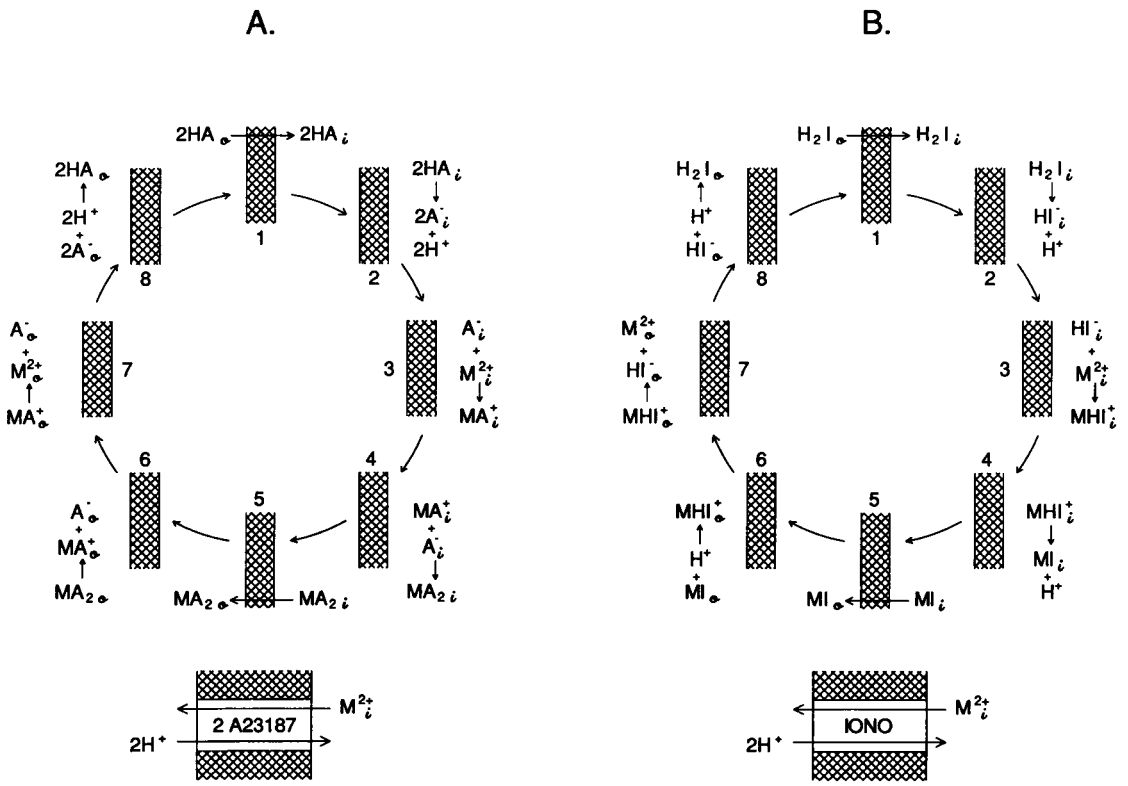

FIGURE 1 The sequential component reactions which comprise the classical transport reactions of A23187 (*A*) and ionomycin (*B*). Hatched areas represent a section of bilayer membrane, and the subscripts *i* and *o* refer to the inside and outside of the bounded volume, respectively. The cycles are written to reflect transport out of a bounded volume.

without further purification. Stock solutions of ionomycin in ethanol were standardized by spectrophotometric titration with $Cu(ClO_4)_2$ that in turn was standardized by titration with primary standard EDTA (Vogel, 1961). Stock solutions of A23187 and 4-BrA23187, also in ethanol, were prepared by weight. Quin-2 (K^+ salt) from Sigma Chemical Co. (St. Louis, MO) was purified by passage over Chelex 100 resin (Bio-Rad, Richmond, CA, 100–200 mesh) in the Cs^+ form. Before use, the resin was washed sequentially with chloroform, acetone, and methanol. Each wash was repeated twice, allowing the resin to stand in solvent for at least 30 min between washes. This was followed by an exhaustive washing with water, conversion to the Cs^+ form using 1 N CsOH, and washing with water until a neutral effluent (pH < 8) was obtained. Cs^+ was selected as the counter ion for Quin-2 and the buffer employed because there is no indication that this cation is complexed or transported by these ionophores (Taylor et al., 1983, 1985; Chapman et al., 1990). The CsOH used to generate the Cs^+ form of Chelex was itself passed over a Chelex column (H^+ form) before use for generating the Chelex (Cs^+) to be utilized when purifying Quin-2. This step largely removed the small amounts of Ca^{2+} and other cations that were present as contaminants in commercial CsOH and thereby reduced the presence of these cations in the Chelex (Cs^+). Omission of this step resulted in unacceptable levels of Ca^{2+} in the purified Quin-2, which was carried through the vesicle preparation procedure (see below), producing final preparations in which the entrapped Quin-2 was 10–15% occupied by Ca^{2+}. Inclusion of this step reduced the Ca^{2+} contamination to <1% of Quin-2 (see Results).

Preparation and characterization of phospholipid vesicles

Freeze-thaw-extruded POPC vesicles were prepared as described by Mayer et al. (1986), with modifications (Chapman et al., 1990; 1991). Briefly, 250 mg of POPC in chloroform was dried by rotation under a nitrogen stream, to produce a film on the wall of a 25 × 150 mm culture tube. Residual solvent was removed under high vacuum (4 h), and the film was subsequently hydrated in 5 ml of buffer containing 10.0 mM HEPES adjusted to pH 7.00 with Chelex-treated CsOH. The buffer contained, in addition, 5 mM Quin-2 (purified and converted to the Cs^+ salt as described above) or 5 mM of $CaCl_2$. The mixture was vortexed until the entire film was suspended and the resulting MLV were frozen in a dry ice-acetone bath, thawed in lukewarm water, and vortexed again. The freeze-thaw and vortexing procedure was repeated 2 times. After this, the MLV were extruded 3 times through two stacked 0.1 μm polycarbonate membrane filters. This step was followed by 6 additional freeze-thaw cycles and 8 additional extrusions. The resulting preparations, referred to as LUVET (Hope et al., 1985), were then applied to Sephadex G-50 minicolumns to remove extravesicular Quin-2 or $CaCl_2$ salts (Fry et al., 1978). The columns were eluted by low-speed centrifugation (Fry et al., 1978) and were equilibrated previously with buffer at the concentration utilized in the lipid film hydration step. A single pass over such columns effectively removes external indicator or $CaCl_2$ (Chapman et al., 1990).

The nominal concentration of POPC in the final preparations was normally 70–90 mM as determined by measurements of lipid phosphorus (Bartlett, 1959). Average vesicle diameters and size distributions were calculated from measurements made on electron micrographs of freeze-fractured samples (Van Venetie, 1980). 100–200 half-shadowed images were measured for each analysis. The average vesicle diameter observed was near 70 nm with a distribution range of ~30 to ~105 nm (Chapman et al., 1990, 1991). These parameters were unaffected by the composition of the hydrating buffer. The assumption that the concentrations of solutes trapped in vesicles prepared by the freeze-thaw extrusion method are the same as those in the hydrating buffer has been shown recently to be invalid, particularly at low solute concentrations and when permeant ion pairs are present (Chapman et al., 1990, 1991). Accordingly, these parameters were determined directly when required. The entrapped volume was calculated as described before (Chapman et al., 1990), whereas the Ca^{2+} content was determined by atomic absorption measurements subsequent to dispersing the vesicles in 0.1 M HCl. The content of entrapped Quin-2 was ascertained by spectrophotometric titration with standard $CaCl_2$ (standardized by titration with primary standard EDTA), after dispersion of the vesicles in deoxycholate (see Results). For ease of reference, some vesicle properties of interest are summarized in Table 1.

The vesicles were prepared at room temperature and stored on the shelf with protection from the ambient light. They were normally used within one week, although the content of entrapped solutes was stable for longer periods. Previous work has indicated that these vesicles can tolerate a 50–60 mOsm osmotic pressure imbalance (internal value high) without lysing or leaking during extended storage (Chapman et al., 1991).

Determination of Ca^{2+} transport kinetics and data analysis

Ionophore-catalyzed transport of Ca^{2+} into or out of POPC vesicles was determined by monitoring formation of the Quin-2:Ca^{2+} complex spectroscopically. For Ca^{2+} uptake, Quin-2-loaded vesicles were employed with $CaCl_2$ salt present at an appropriate concentration in the external medium. Release experiments utilized $CaCl_2$-loaded vesicles and an external Quin-2 concentration of 150 μM. Absorbance measurements were made in an Aminco DW2a spectrophotometer, operated in the dual wavelength mode, using sample and reference wavelengths of 264 and 338 nm, respectively (Ca^{2+} uptake), or 360 and 440 nm, respectively (Ca^{2+} release). In both cases the reference wavelengths are at an isosbestic point in the Quin-2/Quin-2:Ca^{2+} complex difference spectrum. Different wavelengths were used to monitor uptake and release to optimize the signal to noise ratio in both cases. The conditions required for this are different because the Quin-2 concentration (nominal) in the Ca^{2+} uptake experiments was about 1/6 of that used when investigating Ca^{2+} release. In the case of Ca^{2+} uptake, an Oriel No. 59800 band pass filter was placed between the cuvette holder and the beam scrambler-photomultiplier assembly on the DW2a to prevent detection of fluorescent light emitted by Quin-2. Ca^{2+} uptake experiments were initiated with the aid of a rapid mixing device that was designed and constructed in the Hormel Institute shops. This unit delivers two solutions from manually driven syringes to a T-tube mixer and subsequently to a NSG No. T-59FL micro flow cell having a 1 cm path length and a volume of 0.5 ml. Effluent from the flow cell is collected by a third syringe to produce back pressure within the system. Each push drives 3.0 ml through the flow cell such that the preexisting cuvette contents are flushed out before the final 0.5 ml experimental volume is delivered. The entire volume delivered per push is contained previously within the lines that connect the sample syringes to the T-tube, and these lines are contained within a flow-through water jacket to provide for temperature equilibration before mixing. Experiments were conducted at 25°C with a final POPC concentration of 1.5 mM (nominal). POPC plus ionophore was contained within one syringe, whereas $CaCl_2$ was contained in the second. For Ca^{2+} release experiments, the mixing device was not used, and conditions were confined to those accessible to a manual time frame. This was necessary because of problems related to low ionophore solubilities in the absence of POPC.

TABLE 1 Physical properties of the POPC vesicles[a]

Property	Value
Average diameter	70 nm
Entrapped volume (at 1.5 mM POPC)	3.03 μl/ml
POPC molecules/vesicle	
a) Total	41,400
b) Outer monolayer	22,500
c) Inner monolayer	18,900
Internal Quin-2 concentration	9.8 ± 0.7 mM (n = 7)
Internal Ca^{2+} concentration	16.1 ± 0.7 mM (n = 4)
Internal Cs^+ concentration (Quin-2-loaded vesicles)	64 ± 4 mM (n = 7)

[a] The values were determined as described in Materials and Methods or were calculated under the assumptions discussed in Chapman et al. (1990). The internal solute concentrations presented assume no binding to the inner membrane surface.

Data were collected on disk, through a microcomputer interfaced to the spectrophotometer, utilizing the commercial software Unkel Scope (Unkel Software, Inc., Lexington, MA). The sampling rate was varied from 0.1 to 5 s according to the level of ionophore employed. Data were then converted to ASCII files for further analysis. An initial evaluation of the rapid mixing device was conducted using absorbing solutions. These studies demonstrated that the time required to completely replace the cuvette contents with a new solution having a different absorbance is ~300 ms. Dilution experiments showed that mixing afforded by the T-tube assembly is complete within this time and that the DW2a parameters utilized (chopper speed 250 Hz, electronic response time 100 ms) are not factors limiting response time within the overall system. It was further determined, by calculation, that the time required for samples to pass from the T-tube to the cuvette is ~30–40 ms. Based upon these findings, 0.5 s was allowed to pass between completion of sample flow and the onset of data collection. The data analysis procedures utilized require knowledge of sample absorbance at $t = 0$ (the time at which mixing occurs). This parameter was estimated by fitting progress curves to the expression

$$A_T = A_1 e^{-k_1 t} + A_2 e^{-k_2 t}, \quad (1)$$

where A_T is the total absorbance, t is time, and A_1, A_2, k_1, and k_2 are constants that reflect the shape of the curves (the suitability of this type of expression for representing overall progress curves is demonstrated in Results). The initial absorbance (A_0) is then given as the sum of A_1 and A_2. All fitting procedures were based upon the nonlinear least-squares approach. Uncertainty in the values of A_0 arising from the unknown mixing kinetics and the potential for reaction to proceed during mixing was not a significant factor affecting analysis. This was determined by comparing results obtained from selected experiments when slightly differing values of A_0 were assumed.

To obtain the initial rates of absorbance change, the early portion of progress curves (first 10–15%) were fit to the expression

$$A_T = A_0 + Bt + Ct^2, \quad (2)$$

where A_T and A_0 are the total and initial absorbance values, respectively, B is the initial rate, C is a correction factor for nonlinearity, and t is time. Values of B obtained from this expression were converted to Ca^{2+} transport rates through use of a calibration procedure that is described in Results. The way in which the transport rate decreases with the extent of transport is also of interest and was examined by fitting larger portions of the progress curves to expressions for first-order, second-order, and biexponential decay. The expressions utilized are given in the Results. All fitting procedures were conducted with the commercial software Enzfitter (Elsevier-BIOSOFT, Cambridge, UK).

Determination of H^+:Ca^{2+} transport ratios and measurement of membrane potential

The mole ratios of H^+ exchanged for Ca^{2+} by the ionophores were determined from simultaneous measurements of Ca^{2+} transport and change in extravesicular pH. The conditions were the same as described above for determination of Ca^{2+} transport kinetics except that the external buffer concentration was reduced to 5 mM and all ionophore additions were manual. A Fisher model 13–620–280 combination pH electrode, a Beckman model 5400 pH meter, and an external strip chart recorder were employed to measure and record the pH change. For these determinations, the electrode was inserted into the cuvette that was mounted in the holder of the dual-wavelength spectrophotometer. The cuvette contents were stirred magnetically with an accessory provided by SLM·Aminco, Inc. (Urbana, IL). The electrode response was calibrated by small additions of standard acid or base, depending upon the direction of Ca^{2+} transport. Points were taken from the continuous recordings of pH and difference absorbance change, and from these data, transport was calculated and expressed versus time. The units used (μM) refer to the extravesicular concentration.

Measurements of membrane potential during Ca^{2+} transport were made with a tetraphenylphosphonium (TPP^+) electrode (prepared as described in Kamo et al., 1979) and a calomel reference electrode mounted in a stirred and thermostated vessel. The conditions were the same as described for the determination of H^+:Ca^{2+} ratios except that the medium contained 3.3 μM TPP^+ as the Cl^- salt.

RESULTS

Validation and characterization of the transport system

Because internal solute concentrations are not fully predictable when vesicles are prepared by freeze-thaw extrusion (Chapman et al., 1990, 1991), and because investigators utilizing Quin-2 in biological systems have noted discrepancies between internal and external approaches to calibration (e.g., Arslam et al., 1985), careful consideration was given to calibration of the present data. Fig. 2 shows titrations of Quin-2 with Ca^{2+} when the indicator is trapped within vesicles in the presence of excess A23187 (internal approach), and when the indicator has been released by the addition of deoxycholate before titration (external approach). The insert in this figure is a summary plot, showing the difference absorbance change as a function of added Ca^{2+}, for the internal and external conditions. The initial relationships are essentially linear (as might be expected in view of the high affinity of Quin-2 for Ca^{2+} at pH 7.0), and there is no significant difference between the internal and external data until the total Ca^{2+} concentration is sufficient to produce approximately 70% of the maximal response. Thereafter, further increases in the Ca^{2+} concentration give a smaller response when Quin-2 is trapped within the vesicle interior. The maximal responses obtained at high Ca^{2+} concentrations, however, are similar. For reasons considered in the Discussion, we take these data to indicate that the initial additions of Ca^{2+} are nearly completely bound by Quin-2, regardless of whether the dye is trapped within vesicles or free in solution. Expressed in a different way, A23187 fully equilibrates external Ca^{2+} with internal Quin-2 until a condition of approximately 70% saturation is attained, but as the Ca^{2+} concentration is increased further, equilibration is incomplete. In view of this situation, we have used the external method to quantitate the amounts of Quin-2 trapped within vesicle preparations.

The maximal spectral change seen with internal Quin-2 and saturating amounts of Ca^{2+} was smaller (about 30%) when the sample was contained within the flow cell from the rapid mixing device than it was when a standard 3-ml cuvette was employed, despite both cells having a 1 cm path length (data not shown). This situation appears to arise because of the demanding nature of these samples from a spectroscopic point of view. At the vesicle diameters and wavelengths employed, these samples are highly scattering. They also emit substantial fluorescent light that varies with the chemical state of Quin-2 and the wavelengths employed. The use of beam masks and a cutoff filter (see Materials and Methods) reduced, but did not eliminate, the differences between the maximal response obtained with the two types of cuvettes (data not shown). Furthermore, calibration experiments like the ones in Fig. 2 could not be readily carried out in the flow cell. In view of these factors, the spectral change observed in the flow cell with high external Ca^{2+} and ionophore

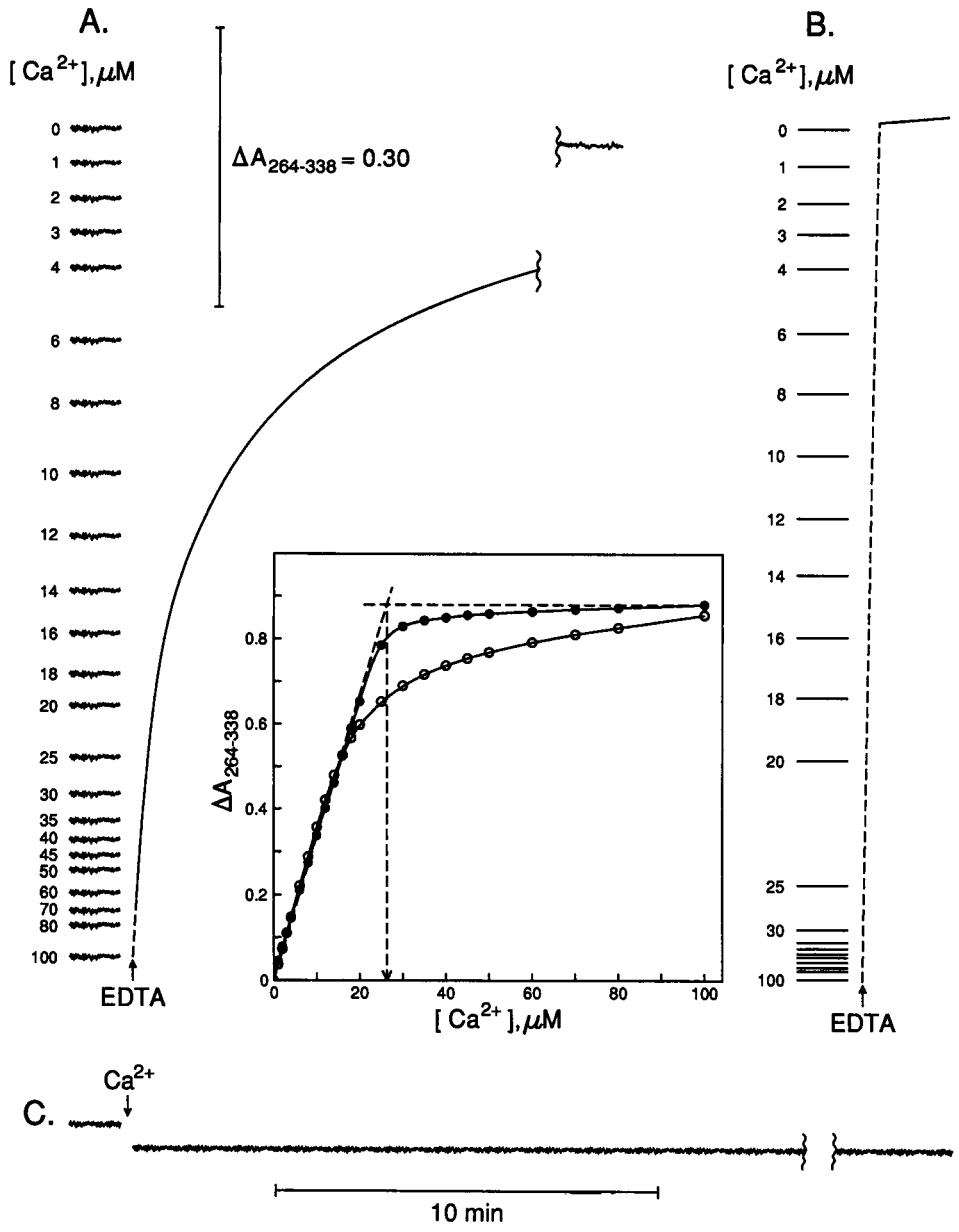

FIGURE 2 Calibration and properties of the vesicle transport system. Quin-2-loaded POPC vesicles were prepared and utilized as described in Materials and Methods. (*A*) Intact vesicles were present at a nominal POPC concentration of 1.5 mM and an A23187 concentration of 4.0 μM; temperature = 25°C. Additions of $CaCl_2$ were made to give the total Ca^{2+} concentrations indicated in the figure. After the difference absorbance at 264 vs. 338 nm had stabilized after an addition of Ca^{2+}, the value was recorded briefly versus time. When the total Ca^{2+} concentration had reached 100 μM, Cs^+-EDTA (pH 7.00) was added at 1.0 mM and the release of internal Ca^{2+} was then monitored continuously. (*B*)An equivalent experiment is shown, except that the vesicles were lysed with 0.33% (w/v) of Cs^+-deoxycholate (pH 7.00) before the additions of Ca^{2+}. The insert panel is a summary plot of the data shown in *A* (○) and *B* (●). Dashed lines in this panel illustrate how the lysed vesicle data were used to determine the amount of entrapped Quin-2. (*C*) Difference absorbance at 264 vs. 338 nm as a function of time for intact vesicle incubated in the presence of 1.0 mM external $CaCl_2$, and in the absence of A23187.

present was taken as the maximal response when calibrating, whereas data obtained with a standard cuvette were relied upon to ascertain the range of linearity and the moles of Quin-2 present in the samples. Values obtained with the two types of cuvettes were interconverted by using a factor calculated from the two observed maximum response values.

Fig. 2 also contains some additional findings that bear upon the precision and interpretation of the kinetic data presented below. After addition of saturating Ca^{2+}, excess EDTA returns the initial difference absorbance reading to near its initial value when the lysed vesicle sample is employed (Fig. 2 *B*). This shows that there is no significant content of Quin-2/EDTA complexable cations present in the vesicle preparations. Without lysing the vesicles, excess EDTA also restores the initial difference absorbance value, which indicates that the A23187 can transport Ca^{2+} out of the vesicles at an appreciable rate, even in the presence of excess internal Quin-2 (Fig. 2 *A*). This shows that forward and back reactions can occur simultaneously and must be considered when interpreting data.

There is no entry of Ca^{2+} into Quin-2-loaded vesicles in the absence of ionophore over time periods that greatly exceed the time frame of these experiments (Fig. 2 *C*), and this was true as well for release of Ca^{2+} from Ca^{2+}-loaded vesicles (data not shown). All transmembrane Ca^{2+} movements are, therefore, ionophore-catalyzed.

Finally, the addition of Ca^{2+} in the absence of ionophore produced a small decrease in difference absorbance, suggesting that a fraction (~5%) of Quin-2 was located in the extravesicular volume (Fig. 2 *C*). This apparent fraction did not increase during vesicle storage (data not shown) and did not increase during transport experiments, as shown by the absence of a significant discontinuity or "absorbance jump" upon adding EDTA to vesicles that had previously been

loaded with Ca^{2+} (Fig. 2 *A*). Furthermore, there was no evidence for an external dye-Ca^{2+} reaction in transport data obtained with the rapid mixing device (see below). This suggests that such a reaction, if occurring, was complete within the mixing time of the instrument, in addition to representing a small fraction of the total Quin-2. In view of these considerations, the potential external dye fraction would not affect data interpretation and, therefore, was ignored in what follows.

Transport parameters considered and methods of data analysis

Fig. 3 shows typical progress curves for the transport of Ca^{2+} into Quin-2-loaded vesicles by A23187, ionomycin, and 4-BrA23187. The concentrations of the ionophores employed have been selected to give approximately equal initial rates of transport and are near the middle of the concentration ranges investigated. Two factors are of interest regarding these curves. First of all, there is little or no initial linear segment, despite the extravesicular Ca^{2+} concentration (1 mM) not being lowered significantly during the experiments (about 10 μM external Ca^{2+} transported in) and despite the linear relationships between Ca^{2+} availability and the response of Quin-2 that were seen in Fig. 2. To obtain the initial rates of transport, it was necessary, therefore, to fit the early segments (10–15%) to Eqs. 1 and 2 and to obtain the initial rates by calculation. Fig. 4 illustrates this procedure for the initial segments of the data shown in Fig. 3. The distribution of residuals about the calculated lines shows that the data are well represented by Eq. 2, and this was the case over the full range of ionophore concentrations investigated. The initial rate values reported below are the means of three to five determinations like those shown in Fig. 3, and these typically agreed within a relative SD of ±5%.

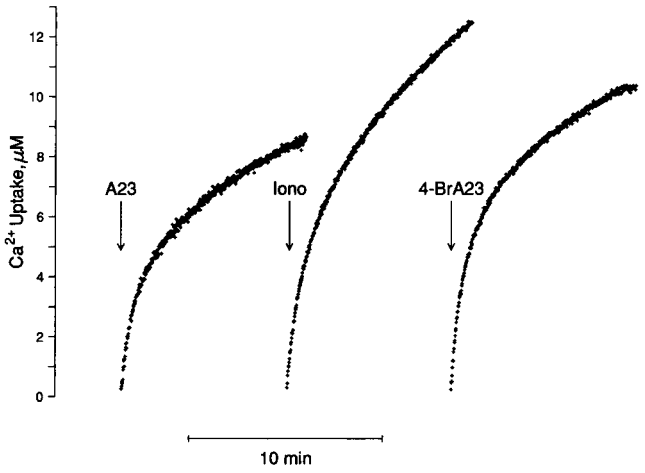

FIGURE 3 Ionophore-catalyzed transport of Ca^{2+} into Quin-2-loaded POPC vesicles. Vesicles loaded with the Cs^+ salts of Quin-2 and HEPES (pH 7.00) were prepared as described in Materials and Methods. During the period of observation, the external medium contained 10 mM Cs^+-HEPES (pH 7.00), 1.00 mM $CaCl_2$ plus 0.125 μM A23187 (*A*), 0.125 μM ionomycin (*B*), or 4.0 μM 4-BrA23187 (*C*). The final concentration (nominal) of POPC was 1.50 mM, and the temperature was 25°C. Before initiation of transport in the flow cell of the rapid mixing device (see Materials and Methods), vesicles plus ionophore were contained in one syringe, whereas $CaCl_2$ was contained in the second. These reagents were initially at twice their final concentrations because mixing diluted them by 50%. Complexation of Ca^{2+} by internal Quin-2 was monitored at 264 vs. 338 nm. Data points were taken at 0.5–1.0 s intervals, and it is the collection of these individual points that is shown in the figure. The 9–13 μM external Ca^{2+} that was transported in during the 10 min observation periods corresponds <50% of the entrapped Quin-2 and, therefore, is well within the linear range of the calibration experiments shown in Fig. 2.

The second point of interest with regard to Fig. 3 is the overall curve shapes, which suggest that different factors limit the rate of transport during early and later periods of individual experiments in a fashion that varies with the ionophore employed. To analyze data in these regards, progress curves where fit to Eqs. 3–5, which are expressions for first order, second order, and biexponential decay, respectively.

$$A = A_m(1 - e^{-kt}) \quad (3)$$

$$A = A_m^2 kt/(1 + A_m kt) \quad (4)$$

$$A = A_{m1}(1 - e^{-k_1 t}) + A_{m2}(1 - e^{-k_2 t}) \quad (5)$$

In expressions 3 and 4, A is the Ca^{2+} transported at time t, A_m is the maximal extent of transport, and k is the rate constant. The designations in Eq. 5 are analogous, with A_{m1}, A_{m2}, k_1, and k_2 referring to the characteristics of the early and later segments of progress curves, respectively. The best fit to experimental data was always obtained with Eq. 5 (Fig. 5 *C*). Rate and extent parameters obtained from this expression are considered individually below.

Ca^{2+} transport as function of ionophore concentration

Fig. 6 shows the relationships between log initial rate of Ca^{2+} uptake into Quin-2-loaded vesicles versus log ionophore concentration for the three compounds in question. A linear relationship is apparent that spans the two to five orders of magnitude in ionophore concentration, which was accessible to investigation with the present procedures. Only in the case of A23187 concentrations higher than ~1 μM or lower than ~10 nM was deviation from linearity observed. For 4-BrA23187 and the linear portion of the data obtained with A23187, the slopes of lines are 1.78 and 1.74, respectively, close to the value of 2 that is expected if these compounds transport through formation of the charge neutral 2:1 (ionophore/cation) complex. Similarly, the ionomycin data show a slope of 0.92, close to the value of 1 expected for transport through formation of the neutral 1:1 complex between Ca^{2+} and that of ionophore.

Analysis of the data according to Eqs. 3–5 produces findings that are less easily rationalized. For all three compounds, the progress curves where best represented as the sum of a rapid but limited first-order process and a slower more sustained one, with both processes beginning simultaneously (e.g., Fig. 5 *C*). The apparent initial rate of the fast process exceeded that of the slow one by ~10-fold, and plots of log initial rate versus log ionophore concentration displayed

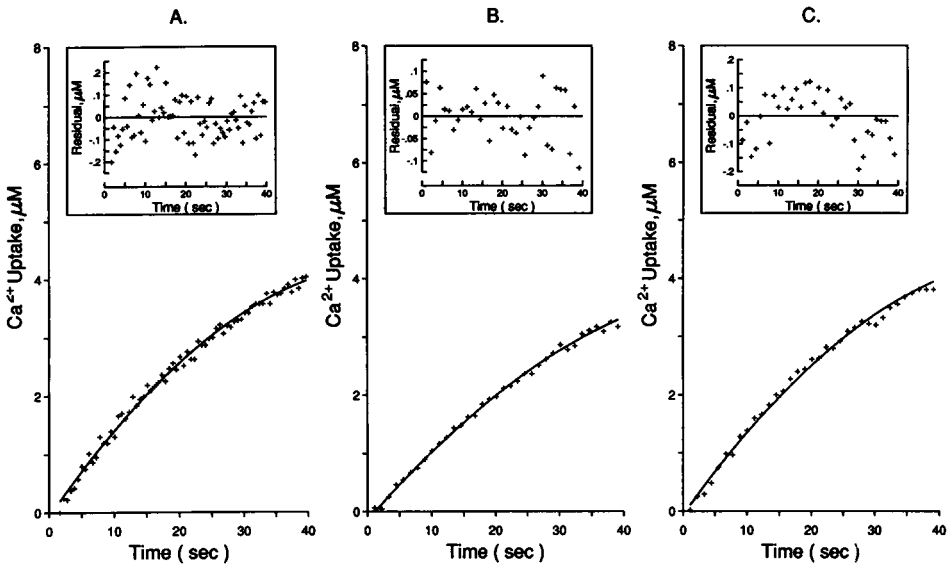

FIGURE 4 Estimation of initial transport rates. The early portions of the progress curves shown in Fig. 3 are shown on an expanded scale, having been fit to Eq. 2 as described in Materials and Methods. The individual points are experimental, whereas the line is calculated using the values of A_o, B, and C (Eq. 2) that were obtained by the fitting procedure. The insert panels are residual plots showing the deviation of individual points from the calculated lines. Panels *A*, *B*, and *C* are data obtained with A23187, ionomycin, and 4-BrA23187, respectively, as described in the legend to Fig. 3.

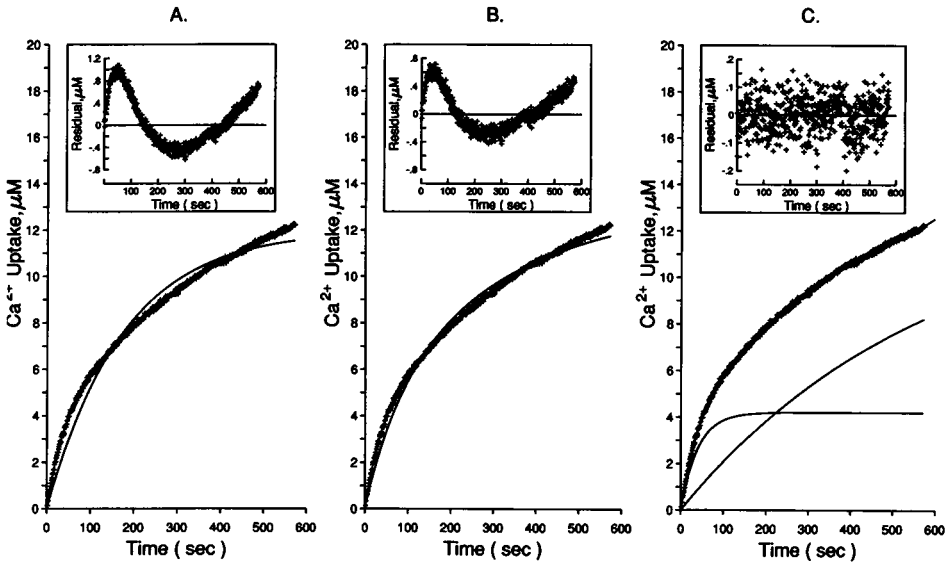

FIGURE 5 Analysis of transport rate decay as a function of reaction progress. The ionomycin data shown in Fig. 3 have been fit to Eq. 3 (panel *A*), Eq. 4 (panel *B*), or Eq. 5 (panel *C*), which are expressions for first-order, second-order, or biexponential decay, respectively (See Results). Individual points are experimental, whereas the lines are calculated using the parameters obtained by the fitting procedure. In panel *C*, the two additional lines are calculated progress curves for transport via the apparent fast and slow processes. The insert panels are residual plots showing the deviation of individual points from the calculated lines. In the case of panel *C*, the residuals are referable to the calculated line representing the sum of the fast and slow processes.

slopes of ~1 in all cases (data not shown). Furthermore, the fraction of Ca^{2+} transported by the two processes (A_{m1} and A_{m2} in Eq. 5) varied, and varied differently with ionophore concentration, and with the ionophore in question. Particularly in the case of A23187, the maximal extent of the fast process (A_{m1}, Eq. 5) was independent of ionophore concentration over much of the range investigated, whereas the comparable parameter for the slow process increased steadily. As a consequence, the calculated sum of these quantities (the maximal extent of transport) was not constant as might be expected if the ionophore were functioning as a simple catalyst, but increased as the ionophore concentration increased (Fig. 7).

The effect of external Ca^{2+} concentration on the initial rate of Ca^{2+} transport

According to the models shown in Fig. 1, A23187 and 4-BrA23187 transport Ca^{2+} through formation of a 2:1 complex (ionophore/cation), whereas with ionomycin, the stoichiometry is 1:1. We have shown previously that during titration of A23187 with Ca^{2+}, the 2:1 species forms first but reacts with excess Ca^{2+} to form two molecules of the 1:1 complex as the Ca^{2+} concentration is increased (Eq. 6; see Chapman et al., 1987).

$$(A23187)_2Ca + Ca^{2+} \rightleftarrows 2(A23187)Ca^{+} \qquad (6)$$

With respect to the effect of Ca^{2+} concentration on the rate of transport, one might then expect a saturation type of curve for ionomycin, whereas with A23187, the rate might rise to a maximum and then decrease as the Ca^{2+} concentration is increased further. With both ionophores, a first-order dependence of transport rate on Ca^{2+} concentration would be expected over the lower Ca^{2+} concentration range. Fig. 8 *A* shows that apparent saturation curves are obtained with both ionophores, which is contrary to expectation in the case of

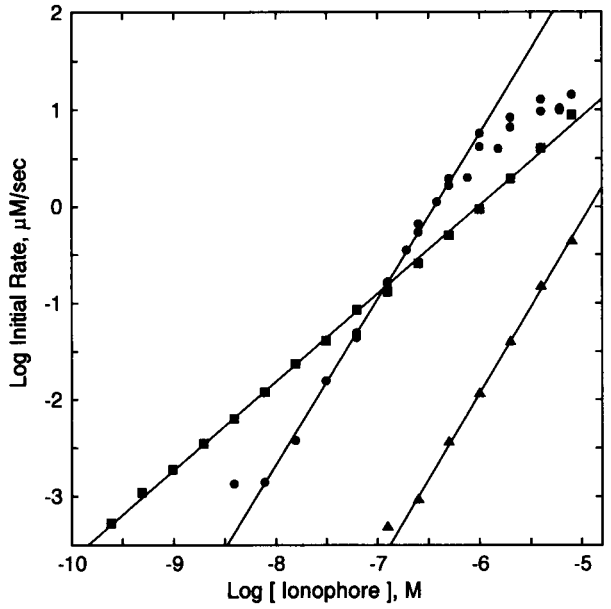

FIGURE 6 Relationships between the initial rate of Ca^{2+} uptake and ionophore concentration. Initial rates were determined as illustrated in Fig. 4 over the indicated ranges of ionophore concentration. Each point represents the mean of three to five determinations with the SDs approximated by the size of the symbols used. (●) A23187; (■) ionomycin; (▲) 4-BrA23187.

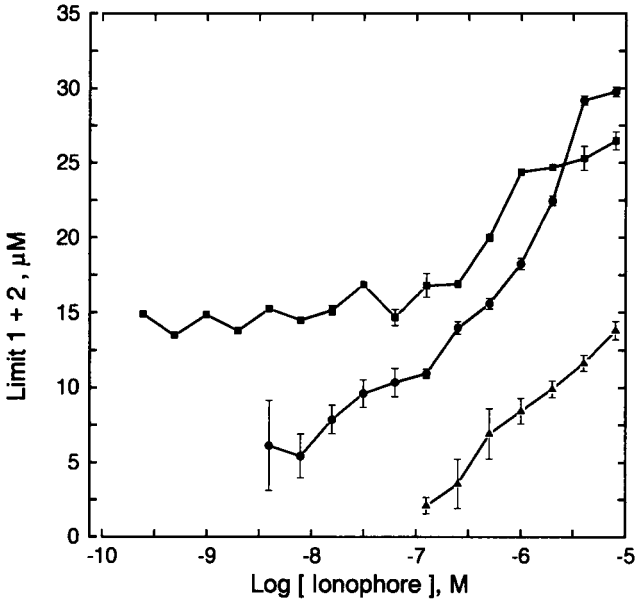

FIGURE 7 The effect of ionophore concentration on the extent of Ca^{2+} transport into POPC vesicles. Progress curves were fit to Eq. 5, as illustrated in Fig. 5 *C*, and the maximal extents of transport were calculated for the two apparent components of these curves. The sums of these quantities are shown in the figure as means of five determinations with an error bar representing the SD. (●) A23187; (■) ionomycin; (▲) 4-BrA23187.

A23187. Log, log plots of these data (Fig. 8 *B*) displayed slopes of ~1 for the lower concentration region, however, consistent with expectation.

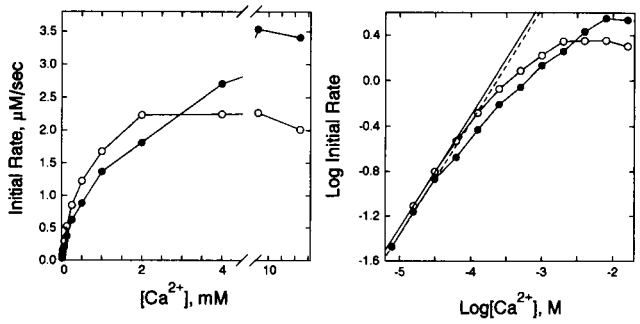

FIGURE 8 The effect of Ca^{2+} concentration on the initial rate of Ca^{2+} transport. (*A*) Initial rates were determined as illustrated in Fig. 4, at external Ca^{2+} concentrations that ranged from 6 μM to 16 mM. The concentrations of A23187 (○) and Ionomycin (●) were 0.50 and 2.0 μM, respectively, selected to give approximately equal rates at 1 mM Ca^{2+} (see Fig. 6). Each point represents the mean of three to five determinations with the symbol size approximating the SDs. Panel *B* shows a log-log plot of these data. The solid and dashed lines have slopes of 1.0 and would be expected to contain all data points for A23187 and ionomycin, respectively.

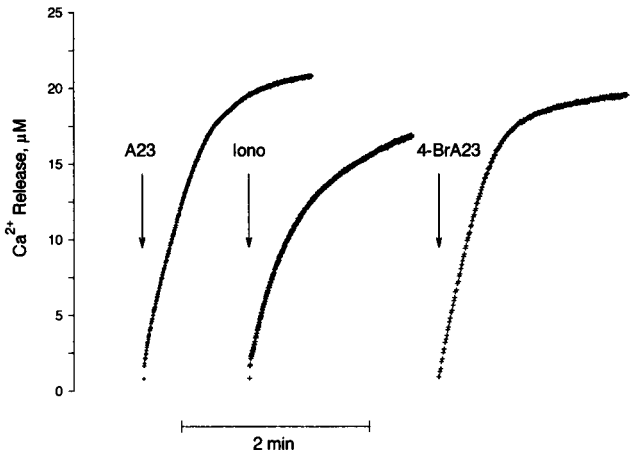

FIGURE 9 Ionophore-catalyzed transport of Ca^{2+} out of $CaCl_2$-loaded POPC vesicles. Vesicles loaded with $CaCl_2$ and the Cs^+ salt of HEPES (pH 7.00) were prepared as described in Materials and Methods. During the period of observation, the external medium contained 150 μM Cs^+-Quin-2, and 10 mM Cs^+-HEPES (pH 7.00), plus 0.500 μM A23187 (*A*), 0.016 μM ionomycin (*B*), or 6.00 μM 4-BrA23187 (*C*). The nominal concentration of POPC was 1.50 mM, and the temperature was 25°C. Ionophore additions were made manually, rather than by rapid mixing, because of the potential for ionophores in water solution to bind to components of the rapid mixing device in the absence of POPC vesicles (ionophore must be added to vesicles when investigating Ca^{2+} release, whereas with Ca^{2+} uptake, Ca^{2+} is added to vesicle-ionophore suspensions). Complexation of Ca^{2+} by external Quin-2 was monitored at 360 vs. 440 nm. Data points were taken at 0.5–1.0 s intervals, and it is the collection of these individual points that is shown in the figure. The 18–24 μM Ca^{2+} that was transported out during the 5 min observation period represents <50% of entrapped Ca^{2+} and corresponds to ~20% of the external Quin-2.

Release of Ca^{2+} from Ca^{2+}-loaded vesicles

When the direction of Ca^{2+} transport is opposite to that employed for the above experiments, the progress curves have distinctly different characteristics, as illustrated in Fig. 9. The

Ca^{2+}-loaded vesicles utilized to investigate transport in the direction of release had ~3 μl entrapped volume/ml of reaction mixture and typically contained enough Ca^{2+} to give a ~50 μM external concentration when all Ca^{2+} was released by detergent lysis (Table 1). The initial internal Ca^{2+} concentration was then on the order of 16 mM, assuming insignificant binding of entrapped Ca^{2+} to the inner surface of the vesicle membranes. Fig. 9 shows that after <1/2 of the entrapped Ca^{2+} is released, transport stops or is slowed markedly. This occurs although a Ca^{2+} concentration gradient of ~5 orders of magnitude continues to exist across the membrane. The initial rate of transport is distinctly more linear than what was seen during Ca^{2+} uptake (compare Figs. 3 and 9), although when viewed on an expanded time scale (analogous to Fig. 4, data not shown), some nonlinearity was still apparent, and it was again necessary to utilize Eqs. 1 and 2 to estimate the initial rates. These values are shown in Fig. 10, over a broad range of ionophore concentration, for all three compounds. Again, the relationships between log rate and log ionophore concentrations are linear. The slopes of these plots, together with those that were obtained for Ca^{2+} uptake, are summarized in Table 2. The values are effectively the same in the case of ionomycin; however, for the other two compounds, the slopes obtained for Ca^{2+} release are clearly higher than the ones for Ca^{2+} uptake. Of further interest are the differences in absolute initial rates that are seen when contrasting transport in the two directions. These are minimal in the case of 4-BrA23187 but marked for A23187, depending upon the ionophore concentration, with Ca^{2+} uptake being faster than release. In the case of ionomycin, a full 20-fold difference is seen across the entire concentration range investigated, with Ca^{2+} release being faster than uptake. These data are not necessarily in conflict with the models shown in Fig. 1; however, they are surprising, given the relative insensitivity of the uptake rate to Ca^{2+} concentrations above 1 mM (Fig. 8) and the fact that conditions should be essentially identical on both sides of the membrane (with the exception of the Quin-2 concentration) during the initial periods of transport.

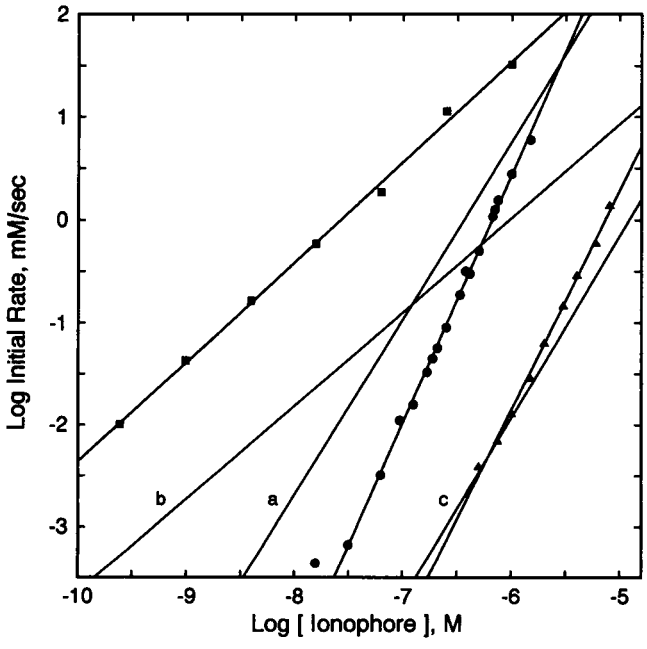

FIGURE 10 Relationships between the initial rate of Ca^{2+} release and ionophore concentration. The initial portions of progress curves like those shown in Fig. 9 were fit to Eq. 2 to estimate initial rates of Ca^{2+} release as a function of ionophore concentration. Each point represents the mean of three to five determinations with the SDs approximated by the size of the symbols used. (●) A23187; (■) ionomycin; (▲) 4-BrA23187. The lines labeled *a*, *b*, and *c* are the fit Ca^{2+} uptake data from Fig. 6 for A23187, ionomycin, and 4-BrA23187, respectively.

TABLE 2 Dependence of initial transport rates on ionophore concentration: slope of the log-log plot

Direction of transport	Ionophore		
	A23187	4-BrA23187	Ionomycin
Ca^{2+} uptake[a]	1.74	1.78	0.92
Ca^{2+} release[b]	2.41	2.14	0.97

[a] Values presented are from the data sets shown in Fig. 6.
[b] Values presented are from the data sets shown in Fig. 10.

Attempts to fit the overall progress curves for Ca^{2+} release to simple expressions such as Eqs. 3–5 failed to identify an expression giving a good representation, in contrast to the case of Eq. 5 and the Ca^{2+} uptake data. Accordingly, the relationship between the extent of Ca^{2+} release and ionophore concentration over a broad concentration range could not be determined in a practical way.

H^+:Ca^{2+} transport ratios and the effect of transport on membrane potential

Regarding the determination of transport mode, data of the types presented so far can support or eliminate specific models such as those shown in Fig. 1, however in general, they cannot prove a particular mechanism and might not detect multiple mechanisms operating simultaneously. To test more rigorously for the possibility of electrogenic transport under the present conditions, the H^+:Ca^{2+} antiport ratios and effects of Ca^{2+} transport on membrane potential were determined directly. Fig. 11 shows that in this system H^+:Ca^{2+} exchange ratios of 2.0 are obtained, within experimental error, for all three ionophores. Measurements of TPP^+ distribution between the bulk aqueous and vesicle phases of these incubations gave no indication of membrane potential formation during the period of net Ca^{2+} transport under conditions were values of <50 mV would have been detected (Fig. 11). However, after maximal Ca^{2+} uptake was obtained, a slow accumulation of TPP^+ was seen in some cases (Fig. 11, *A* and *B*). Similar data were obtained over a range of ionophore concentrations and for transport in both directions (data not shown).

When a potential of ~150 mV, negative inside, is imposed across the membrane before the initiation of Ca^{2+} uptake, data like those shown in Fig. 12 can be obtained. These data show that there is no easily discerned effect of a preexisting potential on the initial rate of Ca^{2+} uptake,

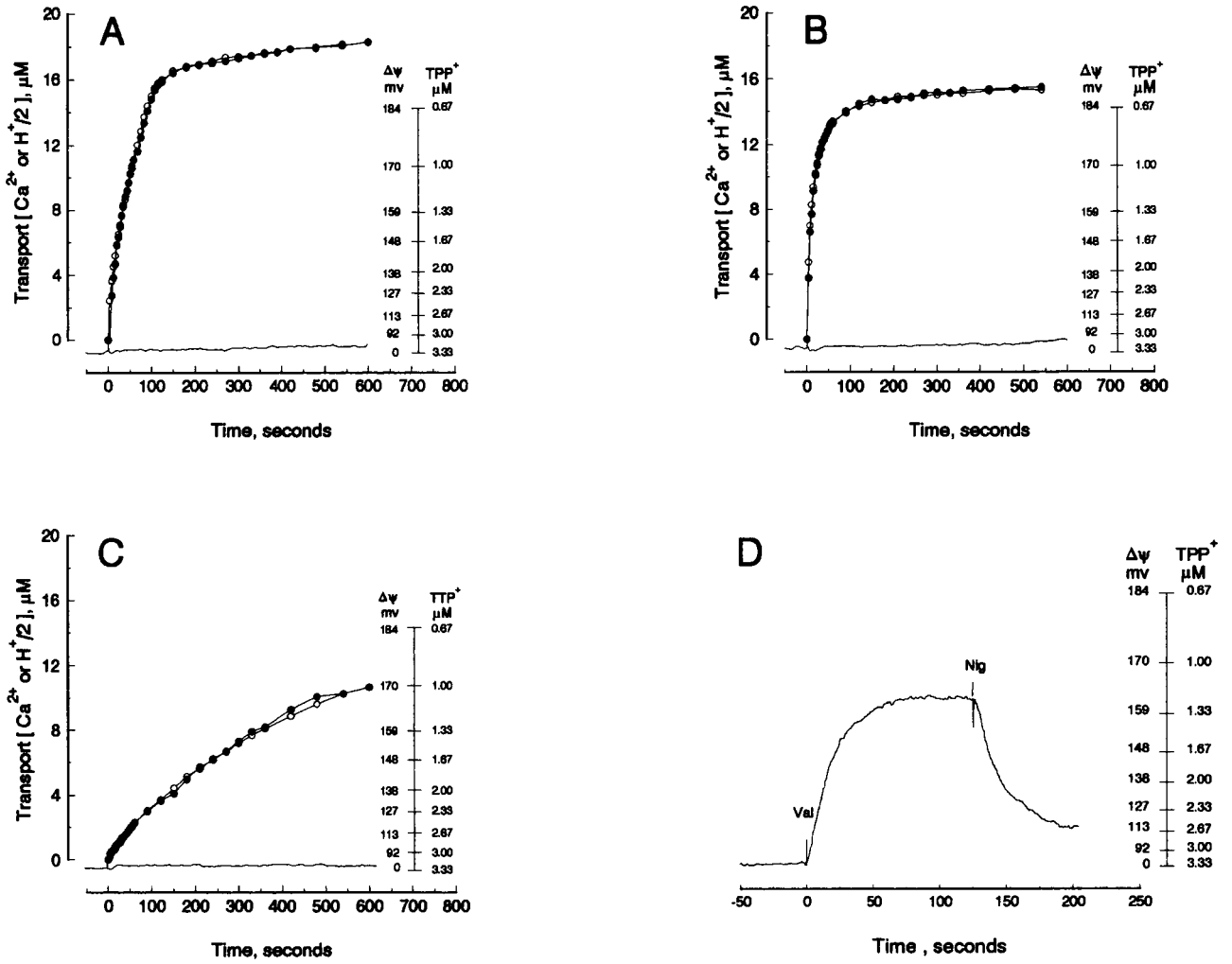

FIGURE 11 Determinations of H^+:Ca^{2+} transport ratios and membrane potential. The data shown in panels *A–C* were obtained with Ca^{2+}-loaded vesicles and are then referable to Ca^{2+} release. The conditions were as described in the legend to Fig. 9 except that the external buffer concentration was reduced to 5 mM to facilitate measurement of the small changes in external pH. Determinations of Ca^{2+} release (○) and H^+ uptake (●) were made simultaneously as described in Materials and Methods. Membrane potential (external TPP^+ concentration) was observed in a parallel experiment using a TPP^+ electrode (see Materials and Methods). In these experiments the external medium contained 3.33 μM TPP·Cl in addition to the other components. The ionophore conditions were as follows: panel *A*, 0.50 μM A23187; panel *B*, 0.063 μM ionomycin; panel *C*, 2.0 μM 4-BrA23187. Panel *D* in this figure is a positive control for panels *A–C* regarding detection of membrane potential by the TTP^+ electrode technique. Vesicles were prepared by the normal procedure except that the medium contained 100 mM KCl instead of $CaCl_2$. External KCl was replaced by 100 mM NaCl during vesicle purification on the sphedex G-50 minicolumns (see Materials and Methods). The additions of valinomycin and nigericin in this panel were 0.20 μM each.

which should accelerate if electrogenic transport occurs (Fasalato and Pozzan, 1989). However, this large potential does produce an enhanced uptake during later stages of the experiments (Fig. 12). Fitting such data to Eqs. 2 and 5, to extract the actual initial rates and extents of transport, respectively, gave the values shown in Table 3. The initial rate is slightly faster in the presence of a membrane potential with ionomycin and 4-BrA23187, and slightly slower with A23187. Comparing the limit data in Table 3 with Fig. 7 illustrates another point of interest. When the internal monovalent cation is K^+ (Fig. 12, Table 3), more Ca^{2+} can be transported into vesicles than when the internal cation is Cs^+ (Figs. 3 and 7). This difference is seen even without an imposed membrane potential and may reflect a greater capacity of these ionophores to catalyze Ca^{2+} for K^+ exchange compared to Ca^{2+} for Cs^+ exchange. The aspects of the data in Fig. 12 and Table 3 related to membrane potential are discussed below.

DISCUSSION

Characteristics of the model transport system and mode of transport

The confidence with which investigators attribute the biological actions of Ca^{2+} ionophores to electroneutral $2H^+$:Ca^{2+} exchange is out of proportion with the strength of the data that indicate that this is the sole activity of these compounds over a range of conditions (see Introduction). Reviewing the literature reveals that structural and solution

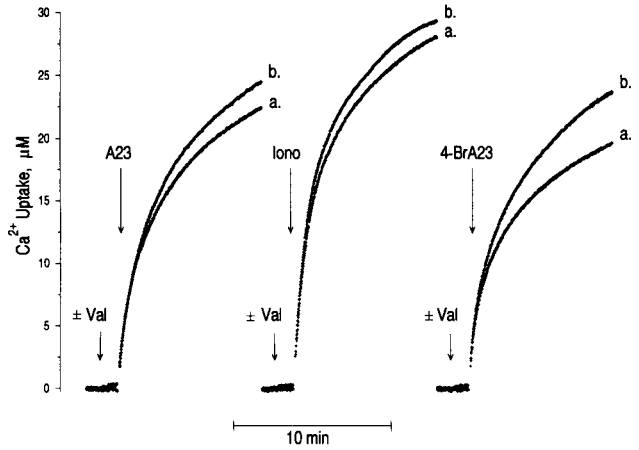

FIGURE 12 The effect of an imposed membrane potential on Ca^{2+} transport. Experiments were conducted as described in the legend to Fig. 3 except that the internal monovalent cation was K^+ rather than Cs^+, whereas the external monovalent was Na^+. When utilized, valinomycin (0.2 μM) was added 60 s before the Ca^{2+} ionophores. Parallel experiments like the one shown in Fig. 11, Panel *D* showed a membrane potential of ~150 mV (inside negative) developed during the 60-s interval and was maintained after the addition of Ca^{2+} ionophores (not shown). A23187, ionomycin, or 4-BrA23187 were added manually where indicated at 0.125, 0.125, or 4.0 μM, respectively. For curves labeled *a*, valinomycin was absent. For those labeled *b*, valinomycin was present.

TABLE 3 The effect of membrane potential on the initial rate and the extent of Ca^{2+} transport[a]

Ionophore	Initial Rate	Limit 1 + 2
	μM/s	μM
A23187		
a) − valinomycin	0.242 ± 0.0005	25.2 ± 0.3
b) + valinomycin	0.230 ± 0.007	27.0 ± 0.3
Ionomycin		
a) − valinomycin	0.354 ± 0.011	31.6 ± 0.3
b) + valinomycin	0.398 ± 0.002	32.4 ± 0.2
4-BrA23187		
a) − valinomycin	0.244 ± 0.009	21.9 ± 0.6
b) + valinomycin	0.260 ± 0.008	27.5 ± 0.6

[a] All values are means ± the SD (n = 5) obtained from experiments like those shown in Fig. 12. Initial rate values were obtained by fitting the progress curves to Eq. 2 as illustrated in Fig. 4. The maximal extents of transport (Limit 1 + 2) were obtained by fitting to Eq. 5 as illustrated in Fig. 5, panel *C*.

chemistry studies of these compounds are substantially more complete than are those that have sought to investigate actual transport, and that solution data are consistent with the existence of electrogenic modes. Investigators have historically utilized bulk two-phase and three-phase solvent systems and effects of ionophores on mitochondria and other subcellular preparations to interrelate the chemical properties and transport activities of these compounds. Bulk solvent systems are inadequate models of phospholipid bilayer membranes and suffer numerous limitations with respect to the types of transport properties which can be investigated by their use. The use of subcellular preparations also results in a lack of experimental flexibility. In addition, it can be difficult to analyze data obtained with subcellular preparations because of interference by the numerous regulated cation-conducting channels and antiporters that they contain. Thus, the early transport data are not only incomplete, but are also of limited value when used in conjunction with chemical data to predict transport characteristics in more complex systems.

In view of the above problems we have sought to develop a flexible and defined model system for investigating transport. The present system is an improvement over earlier vesicle-based systems (e.g., Pohl et al., 1980; Weissman et al., 1980; Blau et al., 1984; Smaal et al., 1985; Utsumi et al., 1985; Shastri et al., 1987; Blau and Weissman, 1988; Sokolove and Kestner, 1989; van Zanten et al., 1992; Walsh and Monbouquette, 1993) in several ways. Preparation of loaded vesicles by freeze-thaw extrusion is straightforward and results in vesicles that are unilamellar, of relatively uniform size, and that are otherwise physically well characterized (Chapman et al., 1990, 1991). The use of POPC as the single phospholipid molecular species produces a bilayer that is fluid over the full range of temperatures utilized with biological systems and allows the transport data to be employed as a reference when investigating effects of lipid composition on transport properties. Vesicles prepared from POPC are stable to storage, rapid mixing procedures, and to a degree of osmotic imbalance. They are also highly impermeant to the indicator used, to metal cations of interest (see Fig. 2), and relatively impermeant to H^+ and OH^- (further discussed below). The use of Quin-2 instead of lower affinity-indicating ligands is advantageous because the extent of transport is increased and the rate of the reverse process is decreased by cation binding to Quin-2. Furthermore, transport can be monitored by conventional dual wavelength UV-VIS spectroscopy or by fluorescence methods, providing the potential for utilizing a wide range of vesicle concentration. The cation complexation chemistry of Quin-2 is well characterized (Tsien, 1980; Tsien et al., 1982; Hesketh et al., 1983) and is largely free of multiple cation-complex stoichiometries, unlike arsenazo III, for example (Ogawa et al., 1980; Dorogi and Newmann, 1981). Preliminary kinetic studies indicate that analogous polyaminocarboxylate ligands, such as EDTA and EGTA, have little effect on the rate of metal ion dissociation from the A23187 complexes of several divalent cations (Thomas, 1991), although the dissociation kinetics of ionomycin complexes with divalent cations (Zn^{2+}, Ni^{2+}) display a first-order dependence on EDTA concentration (Craig, 1990). (Possible effects of the latter finding will be considered below.) Finally, the present system lends itself well to modeling conditions encountered when using ionophores in biological experiments with respect to trapped volume, accessibility of comparable medium conditions, and other properties alluded to above.

The present application of this system constitutes the first fully quantitative demonstration of electroneutral Ca^{2+} transport by these compounds, the data shown in Fig. 11 being particularly revealing in this regard. The H^+:Ca^{2+} exchange ratios are 2.0 as predicted by the model shown in Fig. 1, and

this ratio is obtained in both directions, with all three ionophores, and regardless of whether the absolute rates are fast or slow. Earlier attempts to measure the ratio using planar bilayer membranes (Wulf and Pohl, 1977) and egg phosphatidylcholine vesicles prepared by sonication (Pohl et al., 1980) gave values of zero or H^+ transport ratios that varied with the extent of divalent cation transport. Those unexpected values were thought to reflect a high permeability of the membrane to H^+, relative to the rates of Ca^{2+} flux, or possibly co-transport of an anion by the ionophore (Wulf and Pohl, 1977). No transport of $^{36}Cl^-$ accompanied Ca^{2+} movement in this system (data not shown) and, therefore, the observed H^+ transport occurred via the ionophores.

Although the ratios show that the vast majority of Ca^{2+} transport occurs in exchange for $2H^+$, and is therefore neutral, a small fraction of Ca^{2+} transported electrogenically would have gone undetected by that method. Because of this, measurements of membrane potential were also carried out. Under the conditions described for Fig. 11, *A* and *B* a transmembrane free Ca^{2+} concentration gradient of $\sim 10^5$ exists after release of the cation has attained the maximal extent. If this gradient were electrically equilibrated via complexes such as ACa^+ or $IHCa^+$, a membrane potential of ~300 mV (inside negative) would exist. During the initial period, where net transport occurs, no potential is detected by TPP^+, with a detection limit of 50 mV, again indicating a neutral mechanism in this system. However, as time proceeds beyond that required for maximal Ca^{2+} release, a slow uptake of TPP^+ is observed, amounting to ~0.2 μM over a period of several minutes and corresponding ultimately to a membrane potential of ~75 mV. This potential might reflect a partial electrical equilibration of the Ca^{2+} concentration gradient by charge bearing ionophore complexes, a complete or partial equilibration of the inside acid H^+ concentration gradient that must exist during this time, or a combination of these effects. If one assumes that only Ca^{2+} movements are involved then the maximal rate of electrogenic Ca^{2+} release can be taken as the rate of TPP^+ uptake.[1] That rate corresponds to about 0.01% of the initial charge neutral uptake rate and thus provides an estimate (upper limit) of the relative efficiencies of neutral and electrogenic mechanisms in this system. A comparable estimate was obtained by Moronne and Cohen (1982) using planar bilayers and electrical techniques. These findings contradict the conclusions of Fasolato and Pozzan (1989); however, it is important to note that they reported an inhibition of transport upon collapsing a preexisting potential. The data in Fig. 11 indicate that there is no measurable electrogenic transport when no membrane potential exists initially. To determine whether electrogenic transport can occur when a membrane potential is present, the experiments summarized in Fig. 12 and Table 3 were carried out. The large inside negative potential that existed during these experiments greatly exceeds that which exists across cellular membranes, with the exception of the mitochondrial inner membrane, which has a similar potential of the same orientation. If species such as ACa^+ or $IHCa^+$ could transport electrogenically, one would expect membrane potential to increase the initial rate of Ca^{2+} uptake. Only a small increase was observed in the case of ionomycin and 4-BrA2187, whereas a small decrease was seen with A23187 (Table 3). These findings are in further contradiction with the interpretations of Fasolato and Pozzan (1989), who imply that Ca^{2+} transport by A23187 and ionomycin is substantually electrogenic.

The small initial rate increases seen with 4-BrA23187 and ionomycin may indicate that these compounds have minor electrogenic modes (~10% of total transport) when a high membrane potential is present. However, again such estimates must be taken as upper limits. This is because uncatalyzed H^+ diffusion into the vesicle interior probably occurs when a high inside negative potential is present. The result could be a transmembrane pH gradient, inside acidic, which might accelerate transport via the electroneutral mechanism. We suspect that H^+ permeation accounts for at least a part of the effect of membrane potential on initial rates. We also suspect that H^+ permeation limits the increase in interior pH, as transport proceeds, and that this is partly responsible for the higher extents of transport that are seen when a potential is present.

The initial rate of Ca^{2+} transport

In addition to demonstrating the neutral transport mode of Ca^{2+} ionophores, the present data test aspects of the models shown in Fig. 1 from a broader perspective. They also give some insight into what factors establish the kinetics of transport in this system. These subjects will be considered by discussing the data from the perspectives of initial rate, transmembrane pH gradient, and Ca^{2+} concentration dependence.

From the relationships between log ionophore concentration and log initial rate (Fig. 10, Table 2), it is clear that ionomycin transports via a 1:1 complex, whereas A23187 and 4-BrA23187 transport via 2:1 complexes as has been generally held and depicted in Fig. 1. Slopes of the log/log plots differ from the expected values by small but real amounts, however, and reason for this nonideal behavior remains to be determined.

Perhaps the most interesting aspects of the initial rate data are the differences that are seen when comparing Ca^{2+} uptake and Ca^{2+} release. These are most marked in the case of ionomycin, where Ca^{2+} release is 20- to 25-fold faster than uptake across the full range of ionophore concentration (Fig. 10). These data cannot readily be explained by the difference in Quin-2 concentration that was pointed out in Results, because potential effects of Quin-2 on initial rate kinetics would be appreciable only for ionomycin and should relate to acceleration of Ca^{2+} release from that ionophore. Under the present conditions, this would favor Ca^{2+} uptake over release, the opposite of what is observed. It is also difficult to invoke surface curvature effects as a potential explanation

[1] Transport via the complexes ACa^+ or $IHCa^+$ would produce an H^+:Ca^{2+} exchange, or a net movement of one positive charge per Ca^{2+} transported.

because they generally become negligible for vesicles of greater than ~40-nm diameter. A possible explanation is that the actual transport rates depend critically upon the membrane surface to aqueous phase volume ratio and upon the partition coefficient of the transporting species between the membrane surface, and the actual volume to which it is exposed. If, for example, complexation of Ca^{2+} by ionomycin decreased the partition to the membrane surface, the large difference between the internal and external aqueous phase volumes could easily account for the rapid rate of Ca^{2+} release compared to uptake. It is possible to vary the external and internal surface to aqueous phase volume ratios independently with the present system (external by changing the vesicle concentration, internal by changing the vesicle diameter), and so this possible explanation can be tested.

Another point of interest arises from considering the number of ionophore molecules per phospholipid vesicle that pertain over the ranges of ionophore concentration that have been employed. Using the data in Table 1, these values vary from a high of ~220 ionophore molecules per vesicle to lows of one molecule per ~145, 9, and 0.3 vesicles in the cases of ionomycin, A23187, and 4-BrA23187, respectively. With ionomycin, the log rate versus log ionophore concentration plot is fully linear across this range (Fig. 6). This suggests that ionomycin readily exchanges between vesicles such that the entire population is accumulating Ca^{2+} uniformly, even at the lowest values of ionophore molecules per vesicle. Conversely, the deviations from a linear pattern seen at the lowest concentrations of A23187 and 4-BrA23187 may reflect a lack of rapid ionophore equilibration between individual vesicles. Again, these interpretations should be testable by varying the vesicle concentration.

At A23187 concentrations higher than ~1 μM, the initial rate of transport falls off progressively from the expected value, as shown in Fig. 6. This deviation from the overall linear pattern may reflect the number of turnover cycles that were occurring during the observation period. Typically, only 2–4 μM external Ca^{2+} was transported in during the period used for estimation of initial rates (Fig. 4). As the A23187 concentration rises above 1 μM, the first transport cycle constitutes a growing fraction of this segment. The ionophore distribution between the inner and outer monolayer is likely to be approximately 1:1 before rapid mixing with Ca^{2+}, but this value is likely to change as the number of transport cycles increases, so as to equalize the rate of all transport cycle component reactions (Fig. 1). The initial 1:1 distribution may not be optimal, resulting in lower initial rates than would otherwise be seen.

The influence of transmembrane pH gradient

The calibration data shown in Fig. 2 demonstrate that A23187 cannot always be relied upon to equilibrate external Ca^{2+} with a high affinity chelator contained within a membrane bounded volume. Similar data (not shown) were obtained with ionomycin and 4-BrA23187. It is also seen that under some conditions, the ionophores fail to release all Ca^{2+} from a membrane-bounded volume, even in the presence of excess external chelator (Fig. 9), that the extent of transport can be a function of the ionophore concentration (Fig. 7), and that Ca^{2+} uptake progress curves are not well represented as simple first- or second-order processes (Fig. 5). Because there is no indication that significant electrogenic transport is occurring under the conditions of these figures (membrane potential absent), such findings suggest a dominant role of ΔpH in determining the rate and the extent of transport, even when Ca^{2+} is present in large excess, and a large transmembrane Ca^{2+} concentration gradient exists. For example, considering the nonstoichiometric behavior during the titration of intravesicular Quin-2 with externally added Ca^{2+} (Fig. 2), there are two potential explanations for this behavior, both related to ΔpH. In the first, as the titration proceeds, the internal pH may increase to a point where the ionophore at the internal interface exists predominantly in the anionic form (A^-). Because this form is membrane-impermeant, its accumulation with rising ΔpH could eventually reduce net transport to a negligible rate. In the second explanation, higher internal pH would result in enhanced complexation of free Ca^{2+} as the fraction of ionophore in the anionic form increased. This would result in a progressive replacement of the $2H^+$:Ca^{2+} exchange reaction by Ca^{2+}:Ca^{2+} exchange, thus diminishing the extent of net Ca^{2+} transport.

For the first explanation to be correct, the internal buffering capacity would have to be exceeded during the internal titration experiment. This is because the pK_a of A23187 associated with phosphatidylcholine vesicles is 7.85 (Kauffman et al., 1982; Taylor et al. 1985), and so the internal pH would have to approach 10 for the fraction of internal ionophore in the A^- form to approach 1. The buffer concentration inside these vesicles is not known; however, it is expected to exceed the 10 mM concentration used in the preparation medium by 3- to 3.5-fold, given that the total solute concentration in this medium was 35–40 mM (see Chapman et al. 1990, 1991 for data showing how entrapment effecincy varies with solute concentration and for a discussion of the mechanism by which solutes become concentrated within the vesicle interior). A higher entrapment ratio would be estimated if it were taken from the Cs^+ entrapment data shown in Table 1. If the internal buffer concentration is estimated conservatively at 30 mM, then the nominal concentration of entrapped buffer is about 90 μM, considering that the entrapped volume is 3 μl/ml (Table 1). Taking the pK_a of HEPES to be 7.55, and using the prevailing pH value of 7.0, gives a nominal concentration of entrapped HEPES free acid of ~70 μM. When this value is compared to Fig. 2, it suggests that the internal buffering capacity has not been exceeded at the point where the internal and external titration data begin to deviate (18 μM Ca^{2+} added). Comparing this value to Fig. 7 suggests futher that the observed relationships between the maximal extents of Ca^{2+} uptake and ionophore concentration also cannot be explained by exceeding the internal buffer capacity.

The above considerations focus attention upon the second potential explanation for the lack of equilibration between Ca^{2+} and Quin-2 that is seen in some of the figures. Again considering Fig. 2 as an example, the proposal is that as the concentration of Ca^{2+} added to intact vesicle approaches 18 μM, the rate of the reverse reaction (Ca^{2+} release) progressively increases, such that Ca^{2+}:Ca^{2+} exchange replaces Ca^{2+}:$2H^+$ exchange resulting in no further net transport. This explanation also relates to ΔpH because an increased fraction of internal ionophone in the ionized form will result from even a modest increase in internal pH, whereas the size of this fraction would be an important determinant in establishing the rate of Ca^{2+} release. The internal free Ca^{2+} concentration would be another important determinant, and this value will rise as the fraction of Quin-2 complexed with Ca^{2+} rises during the initial stages of the titration. If this second explanation is correct, one would expect to find a substantial rate of Ca^{2+} release upon adding excess EDTA to stop the forward reaction, and this is observed (Fig. 2, panel *A*). One might also expect that increasing the internal buffer concentration would decrease, but would not eliminate, the differences between internal and external titration data such as those shown in Fig. 2. This was also observed when data obtained with vesicles prepared in 10, 50, and 100 mM HEPES were compared (not shown). Finally, because the rate of the back reaction will depend upon the free concentration of internal cation, one might expect that the affinity of Quin-2 for the transported cation would influence the point at which internal and external titration data begin to deviate. The affinity of Quin-2 for Mn^{2+} and Zn^{2+} exceeds the affinity for Ca^{2+} by about 10^3 (Hesketh et al., 1983). Fig. 13 shows that there is little or no difference between internal titration data obtained with Mn^{2+} or Zn^{2+} and external titration data obtained with Ca^{2+}. Along with supporting the second explanation, the data in Fig. 13 are a strong argument against the inadequate internal buffering explanation, assuming that Mn^{2+} and Zn^{2+} are also exchanged for $2H^+$. It will be necessary to monitor internal pH, together with the parameters determined here, before the relationships between ΔpH and Ca^{2+} transport catalzed by these ionophores can be treated quantitatively.

The influence of Ca^{2+} concentration

A final point of interest relates to the effect of Ca^{2+} concentration on the initial rate of transport by A23187 as shown in Fig. 8. The maximal rate is obtained at a Ca^{2+} concentration near 2 mM, whereas further increases of as much as eightfold are without an additional effect. These results are surprising because preliminary data (not shown) indicate that the formation constant of the ACa^+ complex under comparable conditions is $\sim 30\ \mu M^{-1}$, whereas the available solution chemistry data indicate that the second stepwise binding constant for formation of A_2Ca does not exceed the first one by more than a few-fold (Chapman et al. 1987, 1990). Together, these findings suggest that the rate of transport is maximal in a Ca^{2+} concentration range where effectively all of the external surface ionophore exists as ACa^+ rather than A_2Ca. If further studies show this to be true, then molecules of A_2Ca competent to transport must not be formed as depicted in Fig. 1 *A*, step 4. Two possible alternative formulations are given by Eqs. 7 and 8.

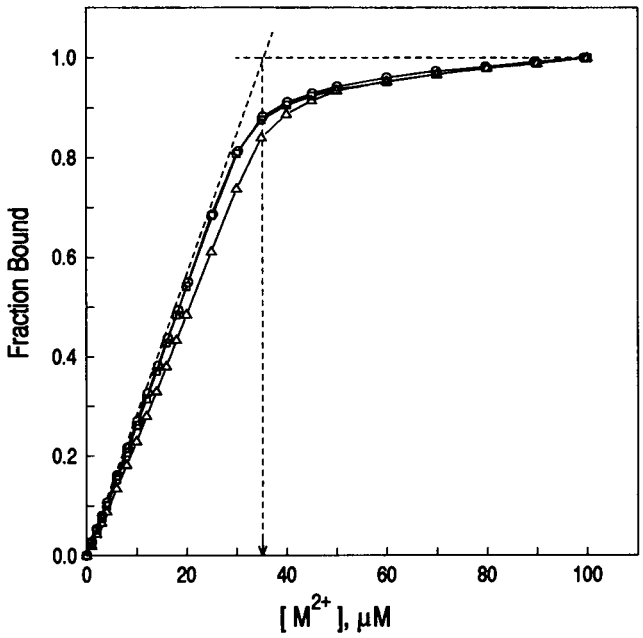

FIGURE 13 Titration of internal Quin-2 with Mn^{2+} and Zn^{2+}. The conditions were the same as those utilized in Fig. 2. (□, △) Intact vesicles were employed, and Quin-2 was titrated with $MnCl_2$ or $ZnCl_2$, respectively, in the presence of 4.0 μM A23187. (○) Lysed vesicles were employed, and Quin-2 was titrated with $CaCl_2$.

$$2\ ACa^+ \rightleftarrows A_2Ca + Ca^{2+} \quad (7)$$

$$ACa^+ + AH \rightleftarrows A_2Ca + H^+ \quad (8)$$

In Eq. 7, both molecules of ACa^+ could be located at the external interface. In Eq. 8, the species HA could be approaching the membrane surface from the interior, returning to the external side after a previous transport cycle. In either case, formation of A_2Ca would have to be coupled with its insertion into the membrane to avoid equilibration with the Ca^{2+} and H^+ concentrations existing in the external aqueous phase. Studies that test these possibilities, and others discussed above, are in progress.

This research was supported by United States Public Health Service Grant HL49181 from the National Institutes of Health, National Heart, Lung and Blood Institute and by the Hormel Foundation. The costs of publication of this article were defrayed in part by the payment of page charges. Therefore, this article must be marked "advertisement" in accordance with 18 U.S.C. Section 1734 solely to indicate this fact.

REFERENCES

Albin, M., B. M. Cader, and W. D. Horrocks, Jr. 1984. Lanthanide complexes of ionophores. 2. Spectroscopic characterization of lanthanide (III) ion binding to lasalocid A and A23187 in methanol. *Inorg. Chem.* 23: 3045–3050.

Albrecht-Gary, A. M., S. Blanc-Parasote, D. W. Boyd, G. Dauphin, G. Jeminet, J. Juillard, M. Prudhomme, and C. Tissier. 1989. X-14885A: an ionophore closely related to calcimycin (A-23187). NMR, thermodynamic, and kinetic studies of cation selectivity. *J. Am. Chem. Soc.* 111: 8598–8609.

Anteunis, M. J. O. 1977. Solution conformation of the ionophore A23187 and its magnesium salt. *Bioorg. Chem.* 6:1–11.

Anteunis, M. J. O., and G. Verhegge. 1981. Solution conformation of calcium-ionomycin. *Bull. Soc. Chim. Belg.* 90:1153–1165.

Antonenko, Y. N., and L. S. Yaguzhinsky. 1988. The ion selectivity of nonelectrogenic ionophores measured on a bilayer lipid membrane: nigericin, monensin, A23187 and lasalocid A. *Biochim. Biophys. Acta.* 938: 125–130.

Arslan, P., F. DiVirgilio, M. Beltrame, R. Y. Tsien, and T. Pozzan. 1985. Cytosolic Ca^{2+} homeostasis in Ehrlich and Yoshida carcinomas. A new, membrane-permeant chelator of heavy metals reveals that these ascites tumor cell lines have normal cytosolic free Ca^{2+}. *J. Biol. Chem.* 260: 2719–2727.

Bartlett, G. R. 1959. Phosphorus assay in column chromatography. *J. Biol. Chem.* 234:466–468.

Blau, L., R. B. Stern, and R. Bittman. 1984. The stoichiometry of A23187- and X537A-mediated calcium ion transport across lipid bilayers. *Biochim. Biophys. Acta.* 778:219–223.

Blau, L., and G. Weissmann. 1988. Transmembrane calcium movements mediated by ionomycin and phosphatidate in liposomes with Fura 2 entrapped. *Biochemistry.* 27:5661–5666.

Bolte, J., C. Demuynck, G. Jeminet, J. Juillard, and C. Tissier. 1982. Étude comparée de troid antibiotiques ionophores: X537A (lasalocide), A23187 (calcimycine) et X14547 A. Complexation des cations IA et IIA, transport de Ca^{++}. *Can. J. Chem.* 60:981–989.

Brasseur, R., M. Notnedame, and J.-M. Ruysschaert. 1983. Lipid-water interface medites reversible ionophore conformational change. *Biochem. Biophys. Res. Commun.* 114:632–637.

Case, G. D., J. M. Vanderkooi, and A. Scarpa. 1974. Physical properties of biological membranes determined by the fluorescence of the calcium ionophore A23187. *Arch. Biochem. Biophys.* 162:174–185.

Chaney, M. O., N. D. Jones, and M. Debono. 1976. The structure of the calcium complex of A23187, a divalent cation ionophore antibiotic. *J. Antibiot.* 29:424–427.

Chapman, C. J., W. L. Erdahl, R. W. Taylor, and D. R. Pfeiffer. 1990. Factors affecting solute entrapment in phospholipid vesicles prepared by the freeze-thaw extrusion method: a possible general method for improving the efficiency of entrapment. *Chem. Phys. Lipids.* 55:73–84.

Chapman, C. J., W. L. Erdahl, R. W. Taylor, and D. R. Pfeiffer. 1991. Effects of solute concentration on the entrapment of solutes in phospholipid vesicles prepared by freeze-thaw extrusion. *Chem. Phys. Lipids.* 60: 201–208.

Chapman, C. J., A. K. Puri, R. W. Taylor, and D. R. Pfeiffer. 1987. Equilibria between ionophore A23187 and divalent cations: stability of 1:1 complexes in solutions of 80% methanol/water. *Biochemistry.* 26:5009–5018.

Chapman, C. J., A. K. Puri, R. W. Taylor, and D. R. Pfeiffer. 1990. General features in the stoichiometry and stability of ionophore A23187—cation complexes in homogeneous solution. *Arch. Biochem. Biophys.* 281:44–57.

Craig, M. E. 1990. Complexation studies of ionomycin with divalent cations and cryptands with lead (2^+) and thallium (+). Ph. D. Thesis, University of Oklahoma, Norman, OK. 280 pp.

Deber, C. M., and D. R. Pfeiffer. 1976. Ionophore A23187. Solution conformation of the calcium complex and free acid deduced from proton and carbon-13 nuclear magnetic resonance studies. *Biochemistry.* 15:132–141.

Divakar, S., and K. R. K. Easwarn. 1987. Conformational studies of A23187 with mono-, di- and trivalent metal ions by circular dichroism spectroscopy. *Biophys. Chem.* 27:139–147.

Dorogi, P. L., and E. Newmann. 1981. Spectrophotometric determination of reaction stoichiometry and equilibrium constants of metallochromic indicators. II. The Ca^{2+}-arsenazo III complexes. *Biophys. Chem.* 13:125–131.

Fasolato, C., and T. Pozzan. 1989. Effect of membrane potential on divalent cation transport catalyzed by the "electroneutral" ionophores A23187 and ionomycin. *J. Biol. Chem.* 264:19630–19636.

Fry, D. W., J. C. White, and D. Goldman. 1978. Rapid separation of low molecular weight solutes from liposomes without dilution. *Anal. Biochem.* 90:809–815.

Hesketh, T. R., G. A. Smith, J. P. Moore, M. W. Taylor, and J. C. Metcalfe. 1983. Free cytoplasmic calcium concentration and the mitogenic stimulation of lymphocytes. *J. Biol. Chem.* 258:4876–4882.

Hope, M. J., M. B. Bally, G. Webb, and P. R. Cullis. 1985. Production of large unilamellar vesicles by a rapid extrustion procedure. Characterization of size distribution, trapped volume and ability to maintain a membrane potential. *Biochim. Biophys. Acta.* 812:55–65.

Kafka, M. S., and R. W. Holz. 1976. Ionophores X537A and A23187 effects on the permeability of lipid bimolecular membranes to dopamine and calcium. *Biochim. Biophys. Acta.* 426:31–37.

Kamo, N., M. Muratsugu, R. Hongoh, Y. Kobatake. 1979. Membrane :Potential of mitochondria measured with an electrode sensitive to tetraphenylphosphonium and relationship between proton electronchemical potential an phosphorylation potential in steady state. *J. Membr. Biol.* 49:105–121.

Kauffman, R. F., C. J. Chapman, and D. R. Pfeiffer. 1983. Location and dynamics of ionophore A23187 bound to unilamellar vesicles of dimyristoylphosphatidylcholine. *Biochemistry.* 22:3985–3992.

Kauffman, R. F., R. W. Taylor, and D. R. Pfeiffer. 1982. Acid-base properties of ionophore A23187 in methanol-water solutions and bound to unilamellar vesicles of dimyristoylphosphatidylcholine. *Biochemistry.* 21:2426–2435.

Kauffman, R. F., R. W. Taylor, and D. R. Pfeiffer. 1980. Cation transport and specificity of ionomycin comparison with ionophore A23187 in rat liver mitochondria. *J. Biol. Chem.* 255:2735–2739.

Krause, G., E. Grell, A. M. Albrecht-Gary, D. W. Boyd, and J. P. Schwing. 1983. Dynamic aspects of complex formation and dissociation between the antibiotic A23187 and alkaline earth cations. *In* Studies in Physical and Theoretical Chemistry. Vol. 24 (Physical Chemistry of Transmembrane Ion Motions). G. Spach, editor. Elsevier, Amsterdam. 255–263.

Liu, C. M., and T. E. Hermann. 1978. Characterization of ionomycin as a calcium ionophore. *J. Biol. Chem.* 253:5892–5894.

Mayer, L. D., M. J. Hope, and P. R. Cullis. 1986. Vesicles of variable sizes produced by a rapid extrusion procedure. *Biochim. Biophys. Acta.* 858: 161–168.

Moronne, M. M., and J. A. Cohen. 1982. Electrical measurement of electroneutral fluxes of divalent cations through charged planar phospholipid membranes. *Biochim. Biophys. Acta.* 688:793–797.

Ogawa, Y., H. Harafuji, and N. Kurebayashi. 1980. Comparison of the characteristics of four metallochromic dyes as potential calcium indicators for biological ;Experiments. *J. Biochem.* 87:1293–1303.

Pfeiffer, D. R., S. M. Hutson, R. F. Kauffman, and H. A. Lardy. 1976. Some effects of ionophore A23187 on energy utilization and the distribution of cations and anions in mitochondria. *Biochemistry.* 15:2690–2697.

Pfeiffer, D. R., and H. A. Lardy. 1976. Ionophore A23187: the effect of H^+ concentration on complex formation with divalent and monovalent cations and the demonstration of K^+ transport in mitochondria mediated by A23187. *Biochemistry.* 15:935–943.

Pfeiffer, D. R., P. W. Reed, and H. A Lardy. 1974. Ultraviolet and fluorescent spectral properties of the divalent cation ionophore A23187 and its metal ion complexes. *Biochemistry.* 13:4007–4014.

Pfeiffer, D. R., R. W. Taylor, and H. A. Lardy. 1978. Ionophore A23187: cation binding and transport properties. *Ann. N. Y. Acad. Sci.* 307: 402–423.

Pohl, W. G., R. Kreikenbohm, and K. Seuwen. 1980. The specificity of ionophore A23187 in cation transport across lipid membranes studies with lecithin vesicles. *Z. Naturforsch.* 23:562–568.

Puskin, J. S., and T. E. Gunter. 1975. Electron paramagnetic resonance of copper ion and manganese ion complexes with the ionophore A23187. *Biochemistry.* 14:187–191.

Puskin, J. S., A. I. Vistnes, and M. T. Coene. 1981. A fluorescence study of A23187 interaction with phospholipid vesicles. *Arch. Biochem. Biophys.* 206:164–172.

Reed, P. W., and H. W. Lardy. 1972. A23187: A divalent cation ionophore. *J. Biol. Chem.* 247:6970–6977.

Reed, P. W., D. R. Pfeiffer, and H. A. Lardy. 1975. Divalent cation transport by antibiotic A23187. *In* Proceedings of the Second Annual New England Bioengineering Conference, R. A. Peura, editor. Vermont University Press, Burlington, VT. 73–80.

Sankaram, M. B., B. P. Shastri, K. R. K. Easwaran. 1987. Interaction of carrier ionophores with phospholipid vesicles. *Biochemistry.* 26: 4936–4941.

Shastri, B. P., M. B. Sankaram, and K. R. Easwaran. 1987. Carboxylic ionophore (lasalocid A and A23187) mediated lanthanide ion transport across phospholipid vesicles. *Biochemistry*. 26:4925–4930.

Smaal, E. B., J. G. Mandersloot, B. deKruiff, and J. deGier. 1985. Essential adaptation of the calcium influx assay into liposomes with entrapped arsenazo III for studies on the possible calcium translocating properties of acidic phospholipids. *Biochim. Biophys. Acta*. 816:418–4227.

Smith, G. D., and W. L. Duax. 1976. Crystal and molecular structure of the calcium ion complex of A23187. *J. Am. Chem. Soc.* 98:1578–1580.

Sokolove, P. M., and M. B. Kester. 1989. Quantitation of Ca^{2+} uptake by arsenazo III-loaded liposomes. *Anal. Biochem.* 177:402–406.

Stiles, M. K., M. E. Craig, S. L. N. Gunnell, D. R. Pfeiffer, and R. W. Taylor. 1991. The formation constants of ionomycin with divalent cations in 80% methanol/water. *J. Biol. Chem.* 266:8336–8342.

Suzuki, K., K. Tohda, H. Aruga, M. Matsuzoe, H. Inoue, and T. Shirai. 1988. Ion-selective polyether antibiotics. *Anal. Chem.* 60:1714–1721.

Suzuki, K., K. Tohda, and T. Shirai. 1987. Natural carboxylic polyether derivatives as lithium ionophores. *J. Chem. Soc. Chem. Commun.* 932–934.

Taylor, R. W., C. J. Chapman, and D. R. Pfeiffer. 1985. Effect of membrane association on the stability of complexes between ionophore A23187 and monovalent cations. *Biochemistry*. 24:4852–4859.

Taylor, R. W., R. F. Kauffman, and D. R. Pfeiffer. 1983. Cation complexation and transport by carboxylic acid ionophores. *In* Polyether Antibiotics. Naturally Occurring Acid Ionophores. Vol. I. J. W. Westley, editor. Marcel Dekker, New York.

Thomas, T. P. 1991. Formation, dissociation and ligand–ligand exchange kinetic studies of ionophore A23187 with divalent cations in 80% methanol-water and vesicle media. Ph. D. Thesis, University of Oklahoma, Norman, OK. 272 pp.

Tissier, C., J. Juillard, D. W. Boyd, and A. M. Albrecht-Gary. 1985. Mode of action of calcimycin (A23187)-II-A study of its interactions with alkali and alkali-earth cations in methanol-water mixtures. *J. Chim. Phys. Phys. Chim. Biol.* 82:899–906.

Tissier, C., J. Juillard, M. Dupin, and G. Jeminet. 1979. No. 98—Mode d'action de la calcimycine (A23187) 1. Équilibre avec les ions alcalins et alcatino-terreux en milieu homogène. *J. Chim. Phys. Phys. Chim. Biol.* 76:611–617.

Toeplitz, B. K., A. I. Cohen, P. T. Funke, W. L. Parker, and J. Z. Gougoutas. 1979. Structure of ionomycin—a novel diacidic polyether antibiotic having high affinity for calcium ions. *J. Am. Chem. Soc.* 101:3344–3353.

Tsien, R. Y. 1980. New calcium indicators and buffers with high selectivity against magnesium and protons: design, synthesis, and properties of prototype structures. *Biochemistry*. 19:2396–2404.

Tsien, R. Y., T. Pozzan, and R. J. Rink. 1982. Calcium homeostasis in intact lymphocytes: cytoplasmic free calcium monitored with a new intracellularly ;Trapped fluorescent indicator. *J. Cell Biol.* 94:325–334.

Utsumi, K., K. Nobori, S. Terada, M. Miyahara, and T. Utsumi. 1985. Continuous fluorometric assay of Ca^{2+} transport by liposomes with Quin2 entrapped: effect of phospholipase A_2 and unsaturated long-chain fatty acids. *Cell Struct. Funct.* 10:339–348.

Van Venetie, R., J. Leunissen-Bijvett, A. J. Verkleij, and P. H. J. T. Ververgaert. 1980. Size determination of sonicated vesicles by freeze-fracture microscopy, using the spray-freezing method. *J. Microscopy*. 118: 401–408.

van Zanten, J. H., and H. G. Monbouquette. 1992. Biomimetic metal-sorbing vesicles: Cd^{2+} uptake by phosphatidylcholine vesicles doped with ionophore A23187. *Biotechnol. Progr.* 8:546–552.

Vogel, A. I. 1961. IV, 20. Determination of copper using fast sulphon black F as indicator. *In* Quantitative Inorganic Analysis, 3rd Ed., Chapter IV. Wiley & Sons, New York.

Walsh, A. J., and H. G. Monbouquette. 1993. Extraction of Cd^{2+} and PB^{2+} from dilute aqueous solution using metal-sorbing vesicles in a hollow-fiber cartridge. *J. Membr. Sci.* 84:107–121.

Weissman, G., P. Anderson, C. Serhan, E. Samuelson, and E. Goodman. 1980. A general method employing arsenazo III in liposomes, for a study of calcium ionophores: results with A23187 and prostaglandins. *Proc. Natl. Acad. Sci. USA*. 77:1506–1510.

Wulf, J., and W. G. Pohl. 1977. Calcium ion-flux across phosphatidylcholine membranes mediated by ionophore A23187. *Biochim. Biophys. Acta*. 465:471–485.